Unexpectedly Similar Charge Transfer Rates through Benzo-Annulated Bicyclo[2.2.2]octanes

Randall H. Goldsmith,[†] Josh Vura-Weis,[†] Amy M. Scott,[†] Sachin Borkar,[‡]
Ayusman Sen,[‡] Mark A. Ratner,*,[†] and Michael R. Wasielewski*,[†]

Department of Chemistry, Argonne-Northwestern Solar Energy Research (ANSER) Center, and International Institute for Nanotechnology, Northwestern University, Evanston, Illinois 60208 and the Department of Chemistry, The Pennsylvania State University, University Park, Pennsylvania 16802

Received January 20, 2008; E-mail: m-wasielewski@northwestern.edu; ratner@northwestern.edu

Abstract: A 4-(pyrrolidin-1-yl)phenyl electron donor and 10-cyanoanthracen-9-yl electron acceptor are attached via alkyne linkages to the bridgehead carbon atoms of bicyclo[2.2.2]octane and all three benzo-annulated bicyclo[2.2.2]octanes. The σ-system of bicyclo[2.2.2]octane provides a scaffold having nearly constant bridge geometry on which to append multiple, weakly interacting benzo π-bridges, so that the effect of incrementally increasing numbers of π-bridges on electron transfer rates can be studied. Surprisingly, photoinduced charge transfer rates measured by transient absorption spectroscopy in toluene show no benefit from increasing the number of bridge π-systems, suggesting dominant transport through the σ-system. Even more surprisingly, the significant changes in hybridization undergone by the σ-system as a result of benzo-annulation also appear to have no effect on the charge transfer rates. Natural Bond Orbital analysis is applied to both σ- and π-communication pathways. The transient absorption spectra obtained in 2-methyltetrahydrofuran (MTHF) show small differences between the benzo-annulated molecules that are attributed to changes in solvation. All charge transfer rates increase significantly upon cooling the MTHF solutions to their glassy state. This behavior is rationalized using combined molecular dynamics/electronic structure trajectories.

Introduction

Covalently linked Donor−Bridge−Acceptor (D−B−A) molecules, where the bridge is comprised of a σ-bond network, have provided a means of elucidating many of the important aspects of intramolecular charge and energy transfer. Saturated spacer groups provided the first unambiguous confirmation of the existence of the Marcus inverted region.[1,2] Bicyclo[2.2.2]octane[3] and norbornane[4] spacers provided early means to determine the distance dependence of intramolecular charge transfer through the incremental increase in the length of an oligomeric bridge group. The utility of these classes of molecules stems from their role as nearly rigid spacers or molecular rods.[5] Despite earlier assumptions about their designation as *inert* spacers,[6] systems containing saturated hydrocarbon bridges have been clearly shown to be electronically relevant to intramolecular charge

transfer[6,7] and to possess a rich electronic structure,[8–11] including interference effects.[12] More recently, the majority of attention has moved away from looking at bridges having all σ-bonds to those with π-bonds. Such a shift was motivated by the increased ability of these π-bridges to convey electronic communication between the π-systems of the D and A groups by maintaining closer energetic resonance, suggested by McConnell's expression for the effective electronic coupling (V_{eff}) between D and A,[13] eq 1,

$$V_{\text{eff}} = \frac{V_{\text{D1}}V_{NA}}{E_1 - E_{\text{D/A}}} \prod_{i=1}^{N-1} \frac{V_{i,i+1}}{E_{i+1} - E_{\text{D/A}}} \tag{1}$$

where V_{ij} are matrix elements between the different subunit wave functions, E_i is the energy of a particular subunit, and the bridge has N equivalent subunits.

The pursuit of greater electronic communication has been driven by the potential development of molecular electronic

† Northwestern University.
‡ The Pennsylvania State University.

(1) Miller, J. R.; Calcaterra, L. T.; Closs, G. L. *J. Am. Chem. Soc.* **1984**, *106* (10), 3047.
(2) Wasielewski, M. R.; Niemczyk, M. P.; Svec, W. A.; Pewitt, E. B. *J. Am. Chem. Soc.* **1985**, *107* (19), 5562.
(3) Leland, B. A.; Joran, A. D.; Felker, P. M.; Hopfield, J. J.; Zewail, A. H.; Dervan, P. B. *J. Phys. Chem.* **1985**, *89* (26), 5571.
(4) Oevering, H.; Paddon-Row, M. N.; Heppener, M.; Oliver, A. M.; Cotsaris, E.; Verhoeven, J. W.; Hush, N. S. *J. Am. Chem. Soc.* **1987**, *109* (11), 3258.
(5) Schwab, P. F. H.; Levin, M. D.; Michl, J. *Chem. Rev.* **1999**, *99* (7), 1863.
(6) Paddon-Row, M. N. *Adv. Phys. Org. Chem.* **2003**, *38*, 1.

(7) Zimmerman, H. E.; McKelvey, R. D. *J. Am. Chem. Soc.* **1971**, *93* (15), 3638.
(8) Beratan, D. N. *J. Am. Chem. Soc.* **1986**, *108* (15), 4321.
(9) Braga, M.; Larsson, S. *Chem. Phys. Lett.* **1993**, *213* (3−4), 217.
(10) Liang, C. X.; Newton, M. D. *J. Phys. Chem.* **1992**, *96* (7), 2855.
(11) Naleway, C. A.; Curtiss, L. A.; Miller, J. R. *J. Phys. Chem.* **1991**, *95* (22), 8434.
(12) Paddon-Row, M. N.; Shephard, M. J. *J. Am. Chem. Soc.* **1997**, *119* (23), 5355.
(13) McConnell, H. M. *J. Chem. Phys.* **1961**, *35*, 508.
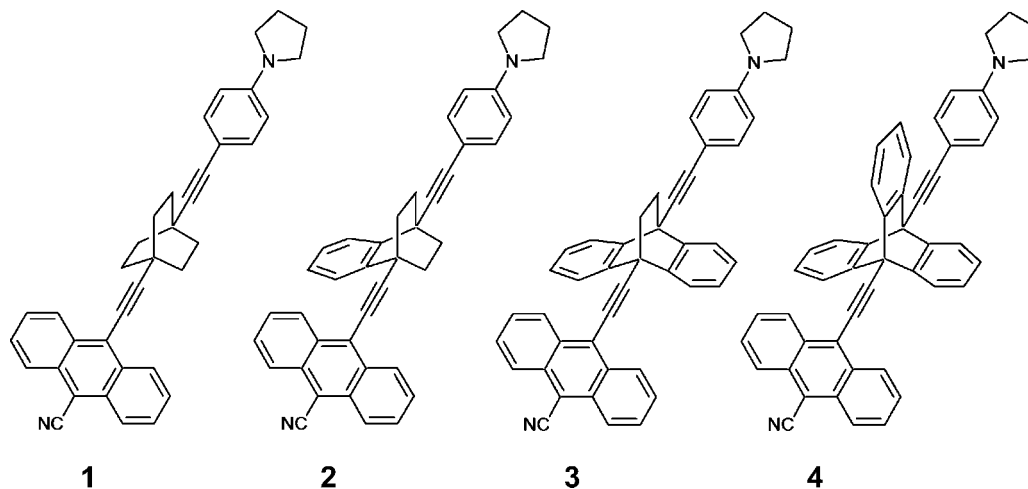
Figure 1. Structures of Donor−Bridge−Acceptor molecules with benzo-annulated BCO bridges.

devices (molecular wires)[14] as well as understanding ultrafast energy and electron transfer in the photosynthetic reaction center and related systems.[15] Studies of π-bridges have revealed qualitatively new transfer regimes that depend on energetic resonance conditions.[16–20] Albinsson and co-workers have recently shown a stark contrast between the efficacy of σ- and π-type bridges by comparing a phenyl group and a bicyclo-[2.2.2]octane group in equivalent positions in a D−B−A system.[21,22] Following the predictions of many earlier experimental and theoretical studies, charge transfer was strongly inhibited by the σ-bridge.

Other recent studies attempting to elucidate ultrafast charge transfer in biological systems have suggested that multiple spatial pathways,[23–26] possibly summing coherently, may contribute to the overall charge transfer rate. As part of our ongoing efforts to understand charge transfer through multiple spatial pathways,[27–29] we have attempted to use the dichotomy between σ- and π-type bridges to develop D−B−A molecules to test predictions about the role of multiple spatial pathways in charge transfer. The σ-system provides a scaffold having nearly constant bridge geometry on which to append multiple weakly interacting π-bridges, so that the effect of incrementally increasing numbers of π-bridges on electron transfer rates can be studied.

For our σ-scaffold, we chose a 1,4-disubstituted bicyclo-[2.2.2]octane (BCO) group. A 4-(pyrrolidin-1-yl)phenyl (PP) electron donor and 10-cyanoanthracen-9-yl electron acceptor (CA) were then attached via alkyne linkages to the scaffold. π-Pathways were then added by replacing the BCO with benzo-annulated BCOs. Up to three π-pathways could be added, with the three-phenyl system comprised of a bridgehead substituted triptycene, as seen in Figure 1. While a few examples of charge and energy transfer systems using asymmetric bridgehead substituted BCO[3,7,30–32] and triptycene[33] bridges have been reported, and many reports have used various benzo-annulated BCO molecules to investigate the relative importance of through-space and through-bond effects,[34,35] to our knowledge, this is the first report to examine charge separation and recombination across the full series of four doubly bridgehead substituted benzo-annulated BCOs.

Experimental Section

Full details regarding the synthesis and characterization of all new compounds can be found in the Supporting Information. Steady-state absorption measurements were performed with a Shimadzu (UV-1601) spectrophotometer. Femtosecond transient absorption measurements were performed using the frequency doubled output of a regeneratively amplified Ti:sapphire laser operating at 2 kHz. The samples were irradiated with $1.0-1.2$ μJ, 416 nm, 120 fs laser pulses focused to a 200 μm diameter spot. The total instrument response time for the pump−probe experiment was 180 fs. The absorbance of all room temperature samples for femtosecond transient absorption spectroscopy was maintained between 0.5 and 0.7 at 416 nm in a 2 mm path length cuvette. Variable temperature studies were conducted using a Janis VNF-100 cryostat with a Cryo-con 32B temperature controller and a

(14) Cuniberti, G.; Fagas, G.; Richter, K. *Introducing Molecular Electronics*; Springer Verlag: Berlin, 2005; Vol. 680.
(15) Wasielewski, M. R. *J. Org. Chem.* **2006**, *71* (14), 5051.
(16) Bixon, M.; Jortner, J. *J. Chem. Phys.* **1997**, *107* (13), 5154.
(17) Davis, W. B.; Svec, W. A.; Ratner, M. A.; Wasielewski, M. R. *Nature* **1998**, *396* (6706), 60.
(18) Davis, W. B.; Wasielewski, M. R.; Ratner, M. A.; Mujica, V.; Nitzan, A. *J. Phys. Chem. A* **1997**, *101* (35), 6158.
(19) Goldsmith, R. H.; Sinks, L. E.; Kelley, R. F.; Betzen, L. J.; Liu, W. H.; Weiss, E. A.; Ratner, M. A.; Wasielewski, M. R. *Proc. Natl. Acad. Sci. U.S.A.* **2005**, *102* (10), 3540.
(20) Weiss, E. A.; Ahrens, M. J.; Sinks, L. E.; Gusev, A. V.; Ratner, M. A.; Wasielewski, M. R. *J. Am. Chem. Soc.* **2004**, *126*, 5577.
(21) Kilså, K.; Kajanus, J.; Macpherson, A. N.; Mårtensson, J.; Albinsson, B. *J. Am. Chem. Soc.* **2001**, *123* (13), 3069.
(22) Pettersson, K.; Wiberg, J.; Ljungdahl, T.; Mårtensson, J.; Albinsson, B. *J. Phys. Chem. A* **2006**, *110* (1), 319.
(23) Balabin, I. A.; Onuchic, J. N. *Science* **2000**, *290* (5489), 114.
(24) Kawatsu, T.; Kakitani, T.; Yamato, T. *J. Phys. Chem. B* **2002**, *106* (43), 11356.
(25) Kuki, A.; Wolynes, P. G. *Science* **1987**, *236* (4809), 1647.
(26) Prytkova, T. R.; Kurnikov, I. V.; Beratan, D. N. *Science* **2007**, *315* (5812), 622.
(27) Goldsmith, R. H.; Wasielewski, M. R.; Ratner, M. A. *J. Am. Chem. Soc.* **2007**, *129* (43), 3066.
(28) Goldsmith, R. H.; Wasielewski, M. R.; Ratner, M. A. *J. Phys. Chem. B* **2006**, *110* (41), 20258.
(29) Weiss, E. A.; Sinks, L. E.; Lukas, A. S.; Chernick, E. T.; Ratner, M. A.; Wasielewski, M. R. *J. Phys. Chem. B* **2004**, *108*, 10309.

(30) Voegtle, F.; Frank, M.; Nieger, M.; Belser, P.; von Zelewsky, A.; Balzani, V.; Barigelletti, F.; De Cola, L.; Flamigni, L. *Angew. Chem., Int. Ed. Engl.* **1993**, *32* (11), 1643.
(31) De Cola, L.; Balzani, V.; Barigelletti, F.; Flamigni, L.; Belser, P.; Vonzelewsky, A.; Frank, M.; Vogtle, F. *Inorg. Chem.* **1993**, *32* (23), 5228.
(32) Zimmerman, H. E.; Goldman, T. D.; Hirzel, T. K.; Schmidt, S. P. *J. Org. Chem.* **1980**, *45* (20), 3933.
(33) Beyeler, A.; Belser, P. *Coord. Chem. Rev.* **2002**, *230* (1−2), 29.
(34) Adcock, W.; Trout, N. A. *Chem. Rev.* **1999**, *99* (5), 1415.
(35) Stock, L. M. *J. Chem. Educ.* **1972**, *49* (6), 400.

Scheme 1[a]
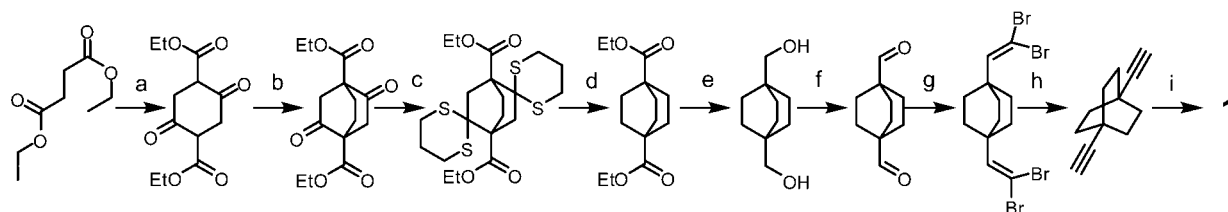
[a] Reagents: (a) KOC_2H_5, EtOH, 55%; (b) (1) NaH, DME, (2) $C_2H_4Br_2$, 71%; (c) $HS(CH_2)_3SH$, $BF_3 \cdot Et_2O$, $CHCl_3$, 80%; (d) Raney Ni, EtOH, 98%; (e) $LiAlH_4$, Et_2O, 89%; (f) oxalyl chloride, DMSO, DCM, quant.; (g) CBr_4, PPh_3, Zn, DCM, hexanes, 53%; (h) *n*-BuLi, THF, 76%; (i) (1) *N*-(4-iodophenyl)pyrrolidine, piperidine, CuI, $Pd(PPh_3)_4$, (2) bromocyanoanthracene, TEA, CuI, $Pd(PPh_3)_2Cl_2$, 9%.

Scheme 2[a]
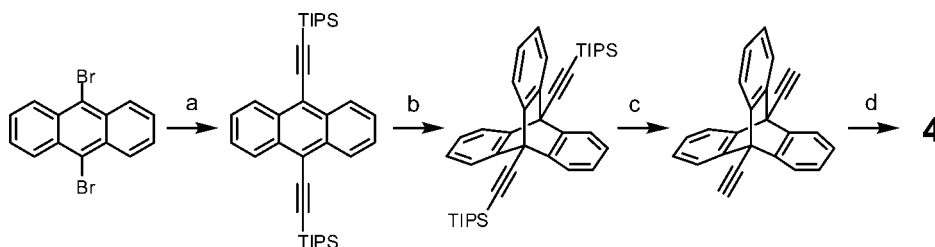
[a] Reagents: (a) TIPS acetylene, DEA, CuI, $Pd(PPh_3)_2Cl_2$, 95%; (b) isoamyl nitrite, anthranilic acid, dioxane, 43%; (c) TBAF, THF, 73%; (d) (1) bromocyanoanthracene, TEA, CuI, $Pd(PPh_3)_2Cl_2$, (2) *N*-(4-iodophenyl)pyrrolidine, piperidine, CuI, $Pd(PPh_3)_4$, 15%.

home-built quartz sample holder with a 1.6 mm path length, so that the sample absorbance at 416 nm was maintained between 0.5 and 0.7. Nanosecond transient absorption measurements were made using a Continuum Panther OPO pumped by the frequency-tripled output of a Continuum 8000 Nd:YAG laser. The probe light in the nanosecond experiment was generated using a xenon flashlamp (EG&G Electrooptics FX-200) and detected using a photomultiplier tube with high voltage applied to only four dynodes (Hamamatsu R928). The total IRF is 7 ns and is determined primarily by the laser pulse duration. The samples for the nanosecond experiments had an absorbance of 0.5−0.7 at 416 nm in a 1 cm path length cuvette. These samples were subjected to four freeze−pump−thaw cycles and excited at either 416 or 430 nm using 2 mJ per pulse (10 Hz) focused to a 5 mm diameter spot size. A full description of the femtosecond transient absorption[36] and nanosecond transient absorption[20] apparatus can be found elsewhere. Transient absorption kinetics were fit to a sum of exponentials with a Gaussian instrument response function by using Levenberg−Marquardt least-squares fitting. Geometry optimizations and single-point calculations were performed using the B3LYP functional with the 6−31G* basis set with Gaussian 98.[37] NBO analysis was performed using the NBO 3.1 add-on[38] with the B3LYP functional and the 6−31G* basis set. Molecular dynamics were performed with MOPAC 2007,[39] employing electronic structure calculations at the AM1/CI level with a 3 electron 2 orbital (HOMO, HOMO−1) active space.

Results

Molecular Design. The donor and acceptor in compounds **1**−**4** were chosen because of their excellent spectroscopic and redox properties, as will be described later, and because they can connect with the bridge via an alkyne linkage, which may be capable of conveying electronic communication between the D/A and the bridge π-system. The syntheses of **1**−**4** were executed using a building-block approach. Aryl halides of the donor[40] and acceptor[41] were prepared in one step from commercial materials. The synthesis of the ethynylated BCO and benzo-BCO bridges comprised the main synthetic challenge. The diethynyl BCO was prepared using variants of known

procedures employed by Stock,[42,43] Sukenik,[44] Kurreck,[45] Albinsson,[46] and co-workers, Scheme 1. The dialkyne derivative of triptycene was prepared using a modification of the procedure of Michl and co-workers,[47] Scheme 2.

In contrast, the benzobicyclo[2.2.2]octene (BBCO) and dibenzo-bicyclo[2.2.2]octadiene (DBCO) derivatives with alkynes at the bridgeheads were unknown. The preparation of BBCO, Scheme 3, started from dimethyl-1,3-cyclohexadiene-1,4 dicarboxylate, which can be produced in multigram quantities from the corresponding saturated cyclohexyl derivative.[48] The esters were reduced following Chu's procedure,[49] and the alcohols were immediately protected with a *tert*-butyldimethylsilyl (TBDMS) group. Reduction of the esters was necessary at this stage because they deactivated the ring system to a degree that made the diene inert toward a Diels−Alder reaction with benzoquinone and benzyne. The protected diol, however, reacted easily with benzoquinone to form the BBCO core while an attempted reaction with benzyne yielded a complex mixture of

(36) Weiss, E. A.; Tauber, M. J.; Kelley, R. F.; Ahrens, M. J.; Ratner, M. A.; Wasielewski, M. R. *J. Am. Chem. Soc.* **2005**, *127* (33), 11842.
(37) Frisch, M. J. et al. *Gaussian 98*, revision A.7; Gaussian, Inc.: Pittsburgh, PA, 1998. Full reference in Supporting Information.
(38) Glendening, E. D.; Reed, A. E.; Carpenter, J. E.; Weinhold, F. *QCPE Bull.* **1990**, *10*, 58.
(39) Stewart, J. J. P. MOPAC 2007; (http://mopac2007.net).
(40) Effenberger, F.; Agster, W.; Fischer, P.; Jogun, K. H.; Stezowski, J. J.; Daltrozzo, E.; Kollmannsberger-von Nell, G. *J. Org. Chem.* **1983**, *48* (24), 4649.
(41) de Montigny, F.; Argouarch, G.; Lapinte, C. *Synthesis* **2006**, (2), 293.
(42) Holtz, H. D.; Stock, L. M. *J. Am. Chem. Soc.* **1964**, *86* (23), 5183.
(43) Baker, F. W.; Stock, L. M. *J. Org. Chem.* **1967**, *32* (11), 3344.
(44) Kumar, K.; Wang, S. S.; Sukenik, C. N. *J. Org. Chem.* **1984**, *49* (4), 665.
(45) Vongersdorff, J.; Kirste, B.; Niethammer, D.; Harrer, W.; Kurreck, H. *Magn. Reson. Chem.* **1988**, *26* (5), 416.
(46) Kilså, K.; Kajanus, J.; Mårtensson, J.; Albinsson, B. *J. Phys. Chem. B* **1999**, *103* (34), 7329.
(47) Caskey, D. C.; Wang, B.; Zheng, X. L.; Michl, J. *Collect. Czech. Chem. Commun.* **2005**, *70* (11), 1970.
(48) Chapman, N. B.; Sotheeswaran, S.; Toyne, K. J. *J. Org. Chem.* **1970**, *35* (4), 917.
(49) Chu, Y. J.; Lynch, V.; Iverson, B. L. *Tetrahedron* **2006**, *62* (23), 5536.

Scheme 3[a]
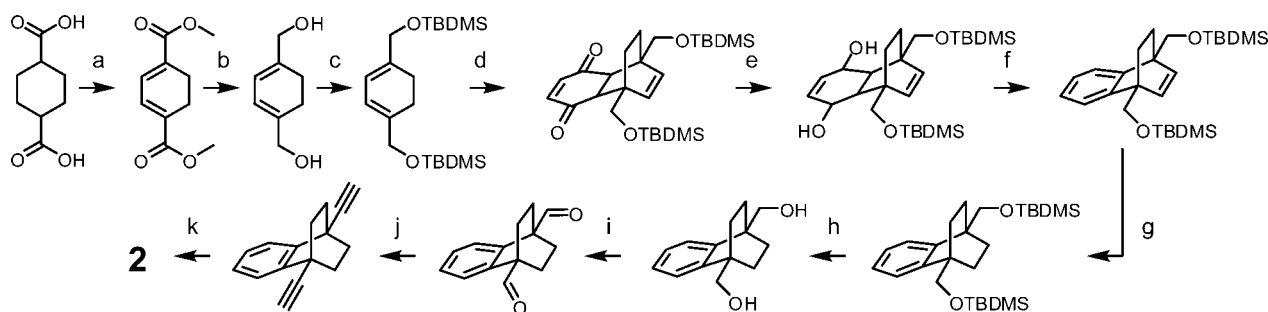
[a] Reagents: (a) (1) $SOCl_2$, Br_2, MeOH, hν, (2) pyridine, 22%; (b) DIBALH, THF, 42%; (c) TBDMSCl, DMF, 66%; (d) *p*-benzoquinone, toluene, 83%; (e) $NaBH_4$, $CeCl_3 \cdot 7H_2O$, MeOH, DCM, quant.; (f) $POCl_3$, pyridine, 68%; (g) H_2, Pd/C, EtOH, EtOAc, 90%; (h) TBAF, THF, 95%; (i) PCC, DCM, 73%; (j) dimethyl-1-diazo-2-oxopropylphosphonate, K_2CO_3, MeOH, 87%; (k) (1) bromocyanoanthracene, TEA, CuI, $Pd(PPh_3)_2Cl_2$, (2) *N*-(4-iodophenyl)pyrrolidine, piperidine, CuI, $Pd(PPh_3)_4$, 5%.

Scheme 4[a]
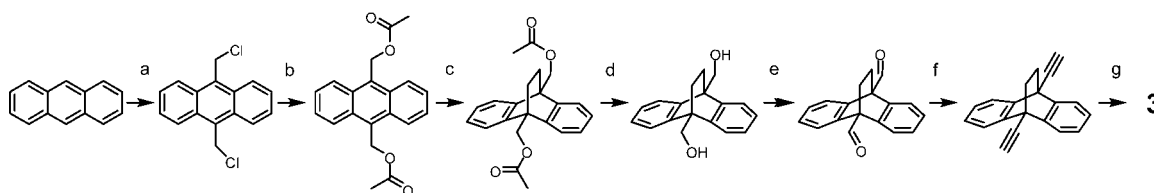
[a] Reagents: (a) paraformaldehyde, $HCl_{(g)}$, dioxane, 50%; (b) NaOAc, HOAc, 78%; (c) toluene, C_2H_4 (2400 psi), quant.; (d) EtOH, KOH, 93%; (e) PCC, DCM, 56%; (f) dimethyl-1-diazo-2-oxopropylphosphonate, K_2CO_3, MeOH, 92%; (g) (1) bromocyanoanthracene, TEA, CuI, $Pd(PPh_3)_2Cl_2$, (2) *N*-(4-iodophenyl)pyrrolidine, piperidine, CuI, $Pd(PPh_3)_4$, 7%.

products. Following procedures of Schmid[50] and Lin,[51] the Diels–Alder adduct was reduced and rearomatized. The remaining olefin was reduced, and the alcohols were deprotected. Arbitrary functionality could be added at this point to the bridgehead positions. To construct the alkynes we first oxidized the alcohols to aldehydes. The Corey–Fuchs procedure failed at this point to produce the desired alkyne. However, application of Bestman's reagent[52] afforded the alkyne directly from the aldehyde in good yield.

Synthesis of the DBCO system, Scheme 4, began with the bis-chloromethylation of anthracene,[53] followed by conversion to the bis-acetoxy derivative.[54] Previous attempts to produce ethanoanthracenes relied on addition of maleic anhydride followed by hydrolysis and bisdecarboxylation with lead tetraacetate.[55] This route is, however, inconsistent and low yielding. The crucial step in our method is Diels–Alder addition of ethene to 9,10-bis(acetoxymethyl)anthracene in toluene[56] in a high pressure autoclave to quantitatively give the corresponding ethanoanthracene derivative. The acetoxy groups were hydrolyzed, and the alcohols were oxidized to aldehydes. The Bestmann reagent was again applied to convert the aldehydes directly to the alkyne.

Sonogashira coupling of the redox active groups to the BCO bridges proved to be difficult, partially because of the reactivities of the D and A aryl halides and partially because of the need to
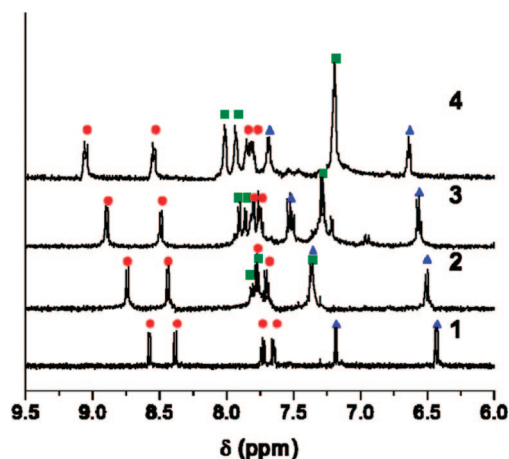
Figure 2. ¹H NMR spectra of the aromatic regions of **1**–**4** at 300 K in $CDCl_3$. Red circles denote peaks from CA, blue triangles denote peaks from PP, and green squares denote peaks from the bridge. Notice the downshifting CA peaks.

asymmetrically substitute the BCO bridge. Other workers[46,57] have reported the successful use of piperidine to couple electron-rich aryl halides to bicyclooctyl or triptycenyl alkynes, and so we attempted using it as the base and/or solvent. Optimization of conditions allowed isolation of the title molecules after purification via preparative HPLC.

The aromatic regions of the NMR spectra of **1**–**4** are shown in Figure 2. As further evidence of the structure, one can see the progressive downfield shift of the protons on the donor and acceptor oriented toward the BCO bridge. As more phenyl groups are fused to the bridge, these protons spend more time caught in the deshielding ring current of the bridge phenyl groups, resulting in this incremental shift downfield.

(50) Schmid, G. H.; Rabai, J. *Synthesis* **1988**, (4), 332.
(51) Lin, C. T.; Wang, N. J.; Yeh, Y. L.; Chou, T. C. *Tetrahedron* **1995**, *51* (10), 2907.
(52) Roth, G. J.; Liepold, B.; Muller, S. G.; Bestmann, H. J. *Synthesis* **2004**, (1), 59.
(53) Miller, M. W.; Amidon, R. W.; Tawney, P. O. *J. Am. Chem. Soc.* **1955**, *77* (10), 2845.
(54) Badger, G. M.; Cook, J. W. *J. Chem. Soc.* **1939**, 802.
(55) Chapman, N. B.; Sotheeswaran, S.; Toyne, K. J. *Chem. Commun.* **1965**, (11), 214.
(56) Meek, J. S.; Godefroi, V.; Wilcox, M. F.; Benson, W. R.; Clark, W. G.; Tiedeman, T.; Evans, W. B. *J. Org. Chem.* **1961**, *26* (11), 4281.

(57) Godinez, C. E.; Zepeda, G.; Garcia-Garibay, M. A. *J. Am. Chem. Soc.* **2002**, *124* (17), 4701.
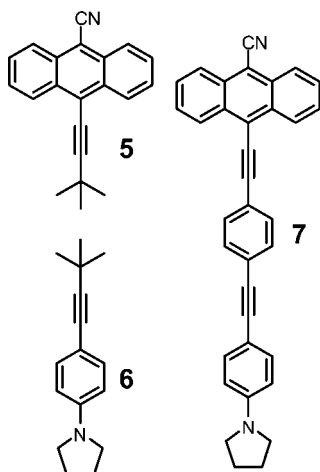
Figure 3. Structures of model compounds.

Table 1. Measured Redox Potentials in V versus SCE and Relevant Electron Transfer Parameters for **1**−**4** in eV

E_{ox}	E_{red}		ΔG_{CS}	λ_I	λ_O	$\Delta G_{CS}^{\ddagger}$
0.74	−1.27	**Toluene**	−0.02	0.21	0.05	0.055
		MTHF	−0.57	0.21	0.72	0.034

Energy Levels. The donor and acceptor were chosen to meet specific redox and spectroscopic requirements and have been used in previous photoinduced electron transfer studies.[58] Compounds **5** and **6** were prepared as appropriate models, Figure 3. Cyclic voltammetry was performed, and the results are summarized in Table 1. These values were used to estimate the energy of the radical pair state by employing Weller's expression,[59] which relies on the Born dielectric continuum model. The free energy change for charge separation, ΔG_{CS}, from the locally excited CA group can then be calculated. To calculate internal reorganization energies for the donor and acceptor, λ_I, we first geometry optimized the neutral species and the appropriate ions of **5** and **6**. Taking the difference in self-consistent field (SCF) energy of the ions calculated in the neutral and ionic geometries yielded λ_I. The solvent reorganization energy, λ_S, was calculated from Marcus' formula[60] assuming a dielectric continuum. Finally, using the classical Marcus expression,[60] the activation barrier for charge separation can be calculated. Results for toluene and MTHF are shown in Table 1, and sample calculations are presented in the Supporting Information.

Spectroscopy. Ground state absorption spectra of **1**−**5** and another model compound, **7** (Figure 3), are shown in Figure 4. The CA acceptor dominates the absorption in this region, although the progressive red shift of the bridge absorption can also be seen. Comparison of **1**−**4** with **5** shows only minimal deviations, showing that the CA acceptor is effectively electronically isolated from the rest of the molecule. Steady-state fluorescence (not shown) is also similar and dominated by the CA acceptor. In contrast, the absorption spectrum of **7** is very different, indicative of significant communication between the donor and acceptor.

Photoexcitation of CA at either 416 or 430 nm results in efficient charge transfer to form the radical ion pair, PP$^{+\bullet}$−B-

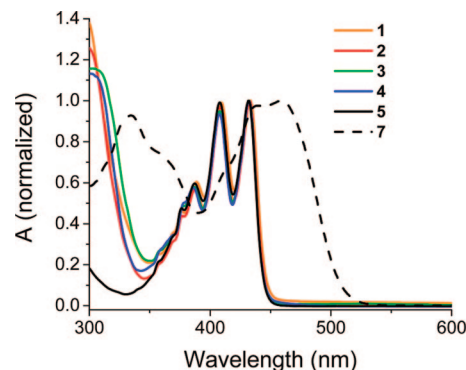(58) Elangovan, A.; Kao, K. M.; Yang, S. W.; Chen, Y. L.; Ho, T. I.; Su, Y. L. O. *J. Org. Chem.* **2005**, *70* (11), 4460.
(59) Weller, A. *Z. Phys. Chem.* **1982**, *130* (2), 129.
(60) Marcus, R. A.; Sutin, N. *Biochim. Biophys. Acta* **1985**, *811* (3), 265.

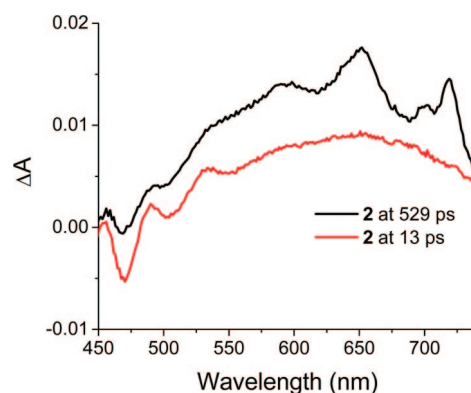**Figure 4.** Steady-state UV−vis spectra of **1**−**5** and **7** in toluene at 295 K.

Figure 5. Transient absorption spectra of **2** at 295 K in toluene.

CA$^{-\bullet}$. The transient absorption spectra are dominated by absorption of ^{1*}CA at early times and CA$^{-\bullet}$ at later times, as shown in Figure 5. The observed CA$^{-\bullet}$ absorption is qualitatively similar to the electrochemically generated anion of a related substituted CA compound.[58] Transient absorption spectra of **5** in toluene shows only ^{1*}CA, while **1**−**4** and **7** show the distinct features of CA$^{-\bullet}$. Transient absorption spectra of **1**−**4** show different λ_{max} values for CA$^{-\bullet}$ in MTHF, while all the spectra are very similar in toluene, Figure 6.

Charge separation (CS) and recombination (CR) dynamics can be examined by measuring the rise and the fall of the CA$^{-\bullet}$ feature. Representative kinetics for **1**−**4** are shown in Figure 7. while time constants for CS and CR are summarized in Table 2. The CS and CR time constants for **1**−**4** in toluene at 295 K are very similar. CS in **7** is comparable to or faster than the instrument response function (τ_{IRF} = 0.18 ps). The CS of **2** and **3** in MTHF at 295 K is marginally slower than that of **1** and **4**. CS times in glassy MTHF at 80 K are faster than those at room temperature, with CS in **1** occurring marginally faster than that in **2**−**4**. CR for **1**−**4** in MTHF at 295 K is too slow to be accurately measured using our ultrafast transient absorption apparatus but too fast to be measured with our nanosecond transient absorption apparatus (τ_{IRF} = 7 ns), although the time constants are all in the range 2−4 ns.

Discussion

Molecules **1**−**4** were designed to show the effect of an increasing number of π-pathways on the rate of charge transfer. Implicit in our design was the assumption that any π-pathway would significantly accelerate charge transfer over a σ-pathway. However, the essentially equal CS and CR rate constants of **1**−**4** show that the π-system has no overall effect, contrary to
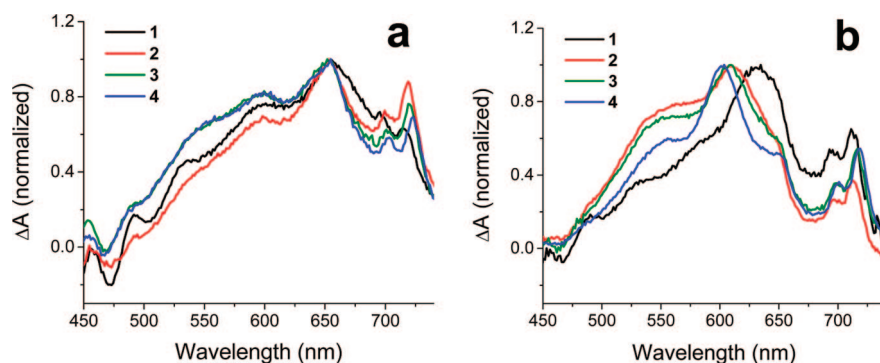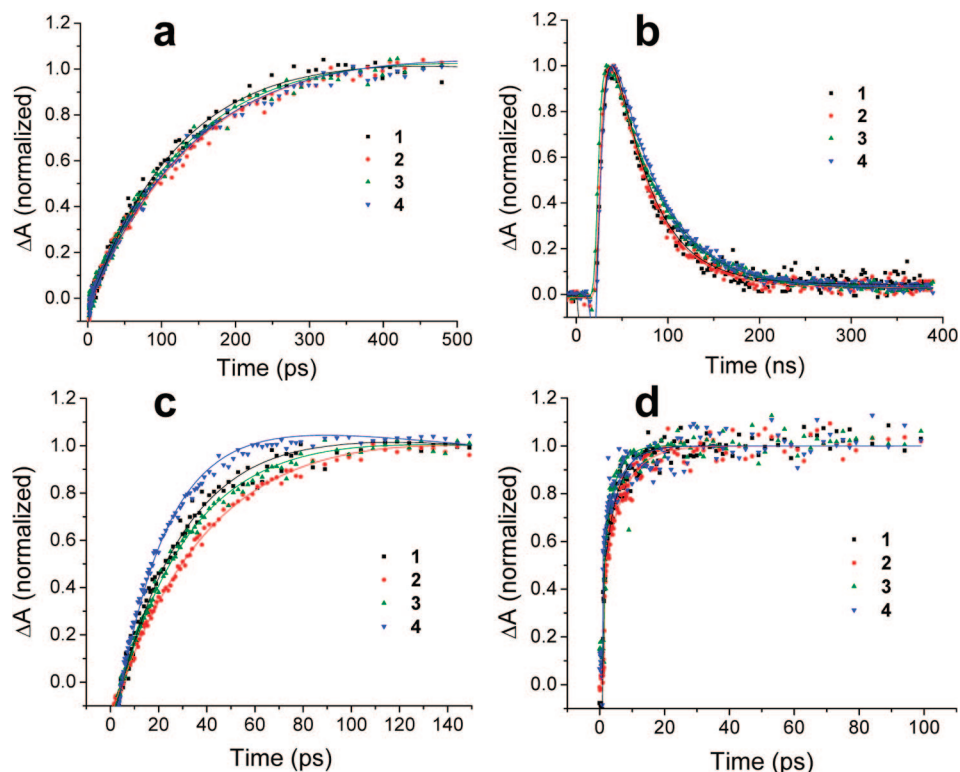
Figure 6. Transient absorption spectra of **1**−**4** at 295 K in (a) toluene at 1029 ps and (b) in MTHF at 239 ps.


Figure 7. Transient absorption kinetics of **1**−**4** measured in (a) toluene at 643 nm at 295 K (CS); (b) toluene at 655 nm at 295 K (CR); (c) MTHF at 613 nm at 295 K (CS); and (d) MTHF at 716 nm at 80 K (CS).

Table 2. Electron transfer time constants of **1**−**4**

	$\tau_{CS(toluene)}$ (ps)	$\tau_{CR(toluene)}$ (ns)	$\tau_{CS(MTHF,300K)}$ (ps)	$\tau_{CS(MTHF,80K)}$ (ps)
1	130 ± 12	48 ± 5	27 ± 3	2.5 ± 1.6
2	145 ± 17	45 ± 5	44 ± 5	6.5 ± 1.0
3	133 ± 5	54 ± 4	33 ± 3	3.9 ± 1.9
4	141 ± 10	55 ± 4	22 ± 4	6.7 ± 2.7

our expectations based on McConnell's expression. Clearly, the relative roles of the π- and σ-systems need to be re-examined.

Contribution of the Bridge π-System. The charge separation rate of **7** was significantly faster than that in **1**−**4**, consistent with our expectations from eq 1 and previous work,[21] showing that a conjugated π-system does provide greater electronic communication than a σ-system in an equivalent geometry. To understand why our nonconjugated π-pathways fail to accelerate k_{CT}, we estimated the respective overlaps of the π system of the chromophores with the π- and σ-systems on the bridge, focusing on nearest and next-nearest neighbor interactions, as

$S_{GTO} = 0.51$ $S_{GTO} = 0.16$

$S_{Exp} = 0.41$ $S_{Exp} = 0.18$

$F_{(i,j)} = -900$ meV $F_{(i,j)} = -22$ meV
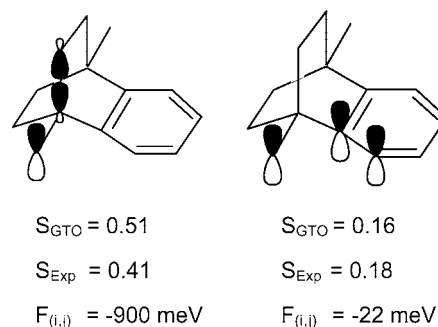
Figure 8. Relevant orbitals for overlap with the bridge σ- and π-systems. S is the spatial overlap, and F is the appropriate Fock matrix element.

shown in Figure 8. We examine the overlap on a per "rung" basis (i.e., though the σ-system has three equivalent σ pathways, we will focus on one at a time where each rung is a set of two methylene carbons) as well as focus on the impact of one additional phenyl ring at a time, as seen in Figure 8. The

proximal alkyne p_π orbital will be considered the only point of communication between the chromophores and the bridge.

Hydrogen-like angular functions were used[61] with two types of radial functions. We used the radial function of the slowest decaying carbon Gaussian-type orbital (GTO) for the 6−31G* basis set. This primitive orbital had a decay constant of 0.48 $Å^{-2}$. We also used a simple exponentially decaying radial function with a decay constant of 1.5 $Å^{-1}$ which was based on the calculated β distance parameter for the through-space distance dependence of electron transfer, 3 $Å^{-1}$.[62] Full calculation details including relevant bond angles are given in the Supporting Information. The overlap between the alkyne p_π orbital and the bridge σ-system is only two to three times larger than the overlap with the marginally more distant π-system, Figure 8. We had hoped that this disparity would be overcome by the more favorable energy resonance condition resulting from the denominator of eq 1 due to the communication being between two π-systems.

We also undertook Natural Bond Orbital[63] (NBO) analysis to probe the significance of the interaction between the more distal π orbitals. By expressing the Fock matrix in the local NBO basis, we can examine the appropriate off-diagonal elements to probe these specific microscopic interactions. Such an approach has been used to great advantage in pathways type analyses of transport in organic molecules.[6,10–12] In addition, direct examination of the matrix element avoids the use of a Mulliken "magic rule" type expression[64] where the matrix element is assumed to be directly proportional to the orbital overlap, eq 2,

$$V_{ij} = \langle \psi_i | H | \psi_j \rangle \propto S_{ij} = \langle \psi_i | \psi_j \rangle \qquad (2)$$

where the Ψ_i refer to the component wave functions.

In contrast to the simple analysis above, the NBO analysis shows a nearly vanishing matrix element between the alkyne and bridge π-systems. Clearly, the application of Mulliken's "magic rule" proportionality is shown to be an inadequate description for our system and suggests caution in the blanket application of eq 2. *The bridge π-system is thus effectively isolated from the π-systems of the chromophores.* Additionally, the isolation of the π-systems is corroborated by measurements of hyperfine couplings of the phosphorus centered radical of X-irradiated 9-phosphinotriptycene.[65] The radical shows no hyperfine coupling to any part of the triptycene and only dipolar coupling to the phenyl hydrogens proximal to the phosphorus.

Contribution of the Bridge σ-System. When examining the significant electronic changes occurring upon benzo-annulation, it is tempting to focus entirely on the π-system. However, the σ-system should also undergo significant electronic changes as the hybridization of the bonding orbitals shifts from sp^3 to sp^2. Specifically, the increasing s character of the orbitals should result in a lower orbital energy. This trend has been seen experimentally via photoelectron spectroscopy in the study of BCO, bicyclo[2.2.2]octene, bicyclo[2.2.2]octadiene, and bicy-
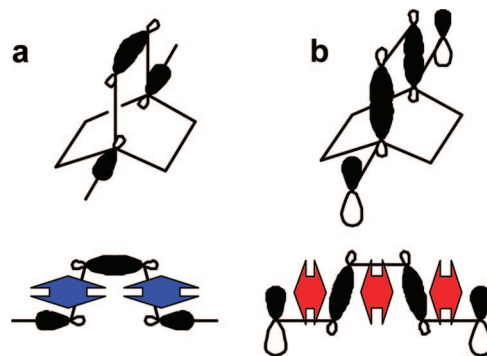

Figure 9. Application of Walton and Adcock's orbital overlap model.[67]

clo[2.2.2]octatriene (barrelene), which showed incrementally dropping σ-system orbital energies from −9.7 to −11.3 eV.[66]

This energy drop is central to the explanation of an important experiment relevant to this work by Walton, Adcock and co-workers, who examined the hyperfine coupling between bridgehead radicals and functionality at the opposite bridgehead in bicyclo[2.2.2]octane and triptycene derivatives.[67] They found significant hyperfine coupling through the bicyclo[2.2.2]octane system to a variety of substituents at the other bridgehead but found no coupling in the triptycene system for any of the substituents. Frequently, it is assumed that hyperfine couplings are communicated to a particular atom via the same superexchange type interactions that mediate electron transfer because the magnitude of the hyperfine coupling is proportional to the local population of the unpaired electron at that nucleus. Consequently, any model proposed for electronic interactions in our system must also be able to accommodate their results. Our expectation was that the π-pathways would *increase* communication between bridgehead anchored donor and acceptor groups. Our experimental result is that the π-pathways have a negligible effect. However, the Walton, Adcock, et al. experiments suggest that the π-pathways *decrease* communication. Coupling is suggested to be mediated via overlap between a series of antiperiplanar sp^3 hybridized orbitals. Such an orientation is optimal for maximum overlap (Cieplak's model).[68,69]

To explain their result, the authors[67] suggest the dominance of an antiperiplanar arrangement of σ-orbitals in which the dominant communication conduit is the σ-bond oriented parallel to the bridgehead radical orbital and the C−H bond of the opposite bridgehead, Figure 9a. The direct through-space interaction between the bridgeheads has been shown to be minimal,[70] while this "skipped" through-bond mechanism (as opposed to going through consecutive bonds) is supported by measurements of hyperfine couplings in related adamantane radicals, where the coupling constants to two geminal hydrogens would be equivalent in the case of consecutive through-bond coupling, but are significantly different due to the presence of antiperiplanar overlap.[71] As mentioned above, fusing the phenyl rings to the BCO changes the hybridization of this bond, removing an energetic resonance condition and decreasing the

(61) DeKock, R. L.; Gray, H. B. *Chemical Structure and Bonding*; University Science Books: Sausalito, CA, 1989.

(62) Paddon-Row, M. N.; Jordan, K. D. *Modern Models of Bonding and Delocalization*; VCH, Weinheim, New York, 1988; Vol. 6.

(63) Reed, A. E.; Curtiss, L. A.; Weinhold, F. *Chem. Rev.* **1988**, *88* (6), 899.

(64) Mulliken, R. S. *J. Phys. Chem.* **1952**, *56*, 295.

(65) Ramakrishnan, G.; Jouaiti, A.; Geoffroy, M.; Bernardinelli, G. *J. Phys. Chem.* **1996**, *100* (26), 10861.

(66) Haselbach, E.; Heilbronner, E.; Schroder, G. *Helv. Chim. Acta* **1971**, *54* (1), 153.

(67) Binmore, G. T.; Walton, J. C.; Adcock, W.; Clark, C. I.; Krstic, A. R. *Magn. Reson. Chem.* **1995**, *33*, S53.

(68) Cieplak, A. S. *J. Am. Chem. Soc.* **1981**, *103* (15), 4540.

(69) Tomoda, S. *Chem. Rev.* **1999**, *99* (5), 1243.

(70) Hoffman, R. *Acc. Chem. Res.* **1970**, *4* (1), 1.

(71) Krusic, P. J.; Schleyer, P. V.; Rettig, T. A. *J. Am. Chem. Soc.* **1972**, *94* (3), 995.

Table 3. Parameters from NBO Analysis[a]

	no phenyl group	with phenyl group
$F_{(1,1)}$	−7317	−7371
$F_{(2,2)}$	−15640	−16402
$F_{(3,3)}$	−15667	−18360
$F_{(1,2)}$	−898	−816
$F_{(1,3)}$	264	218
$F_{(1,4)}$	−41	−33
$F_{(1,5)}$	2.7	2.7
$F_{(2,3)}$	−3237	−3634
$F_{(2,4)}$	−816	−686
	Direct	
V_{eff} 1,5	2.7	2.7
	1 Step	
V_{eff} 1,2,5	4.4	2.9
V_{eff} 1,3,5	8.3	4.3
V_{eff} 1,4,5	4.4	2.9
	2 Step	
V_{eff} 1,2,3,5	11	6.5
V_{eff} 1,2,4,5	−9.5	−5.6
V_{eff} 1,3,4,5	11	6.5
	3 Step	
V_{eff} 1,2,3,4,5	15	9.8
total	47	30

[a] Matrix elements are given in meV. The i,j refer to the numbered orbitals above. $F(i,j)$ refer to the elements of the Fock matrix. $V_{eff}(i,j,...)$ are calculated using eq 1. The model system is symmetric across NBO 3.
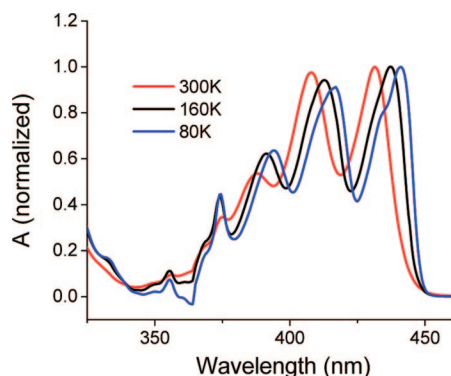
Figure 10. Steady-state UV−vis of **1** at a variety of temperatures in MTHF.

effective mixing, consistent with McConnell's relation, eq 1. This explanation can be conveniently adapted to suit our system geometry, as shown in Figure 9b. Analogously, the *p* orbitals of the alkyne should be in good periplanar overlap with the *σ* bonds originating at the bridgehead, which are in turn in good periplanar overlap with the *σ* bond at the opposite bridgehead, and sequentially the *p* orbital at the opposite alkyne (NBO's 1−2−4−5 in Table 3). Because this model suggests minimal importance for the central *σ* orbital (NBO 3 in Table 3), a change in hybridization of this orbital would be predicted to have a minimal effect on V_{eff}.

NBO analysis for the bonding orbitals of the bridge *σ*-system is summarized in Table 3. The analysis captures the effect of the changing hybridization that accompanies the addition of the phenyl ring by showing a decrease in bonding orbital energy. NBO analysis also captures the dominance of skipped through-

bond mixing over consecutive bond mixing in the antibonding orbitals (not shown), consistent with NBO analysis of BCO anions by Liang and Newton.[10] Charge transfer in our system is likely proceeding via a hole transfer mechanism because the electron acceptor is first locally excited, so we will focus on the bonding orbitals. However, mixing through the bonding orbitals shows a complex network of destructive interference *within each methylene rung*, again consistent with previous work.[10] As a consequence of the destructive interference the NBO analysis predicts that the majority of through-bond communication involves NBO 3. Thus, NBO analysis suggests significant contributions from NBO 3 to the total V_{eff} and an effect from the significant perturbation of that bond accompanying introduction of a phenyl group, and so does not support the models in Figure 9.

Re-examining Walton and Adcock's result, we calculated the hyperfine coupling at the bridgehead hydrogen and found the expected disparity in magnitude between the BCO (hfc$_{BCO-H}$ = 3.2G) and triptycene radicals (hfc$_{Trip-H}$ = −0.18G). However, hyperfine coupling constants to the adjacent bridgehead carbon, which were not observed experimentally, did not show a similar disparity in magnitude (hfc$_{Trip-C}$ = 0.75G, hfc$_{Trip-H}$ = −0.74G). If delocalization of the radical via antiperiplanar overlap was the dominant interaction, one would expect the magnitude of spin density at the carbon and hydrogen to track each other. Delocalization of the unpaired electron is only one mechanism to attain nonvanishing spin density.[72] In the study of [1.1.1]bi-cyclopentane (staffane) *σ* radicals, two mechanisms of spin propagation were identified: spin delocalization and spin po-larization.[73] NBO deletion analysis showed that spin polarization was the dominant mechanism. It is expected to be even more dominant in a BCO system where through-bond and through-space delocalization will be even weaker due to the large distance between bridgeheads. Hyperfine coupling from spin polarization is extremely sensitive to the hybridization of surrounding atoms,[72] with the benzo-annulation consequently having a large effect on the polarization. As a result, we find no conflict with Walton and Adcock's suggestion that the change in hybridization reduces the spin density, only that it is a result of the change in polarization rather than a reduction in delocalization. Most importantly, since it is this delocalization that is most relevant when comparing hyperfine couplings and V_{eff} for charge transfer, these results are likely not in conflict with our observation of unchanging k_{CT}.

Nonetheless, the NBO analysis and photoelectron spectra mentioned above strongly suggest consequences of the changing hybridization for k_{CT}. From a different perspective, one can simply view **1−4** as three-site *π*−*σ*−*π*-systems with the lowest *σ*-orbital energy E_σ = −9.7 eV for BCO in **1** and E_σ = −11.3 eV for triptycene in **4** estimated from the barrelene data.[66] Taking E_π = −7.8 eV from photoelectron spectra of 9-cyanoan-thracene,[74] we can use eq 1 to estimate the difference in V_{eff} going from **1** to **4** to be a reduction by a factor of 0.54, corresponding to a reduction in k_{CT} of 0.29. This reduction can be relaxed significantly by increasing the energy gap between the *π*- and *σ*-systems, and so one origin of our static rates could be underestimation of this gap. Alternatively, eq 1, whose

(72) Wertz, J. E.; Bolton, J. R. *Electron Spin Resonance: Elementary Theory and Practical Applications*; McGraw-Hill: New York, 1972.

(73) McKinley, A. J.; Ibrahim, P. N.; Balaji, V.; Michl, J. *J. Am. Chem. Soc.* **1992**, *114* (26), 10631.

(74) Klasinc, L.; Kovac, B.; Gusten, H. *Pure Appl. Chem.* **1983**, *55* (2), 289.
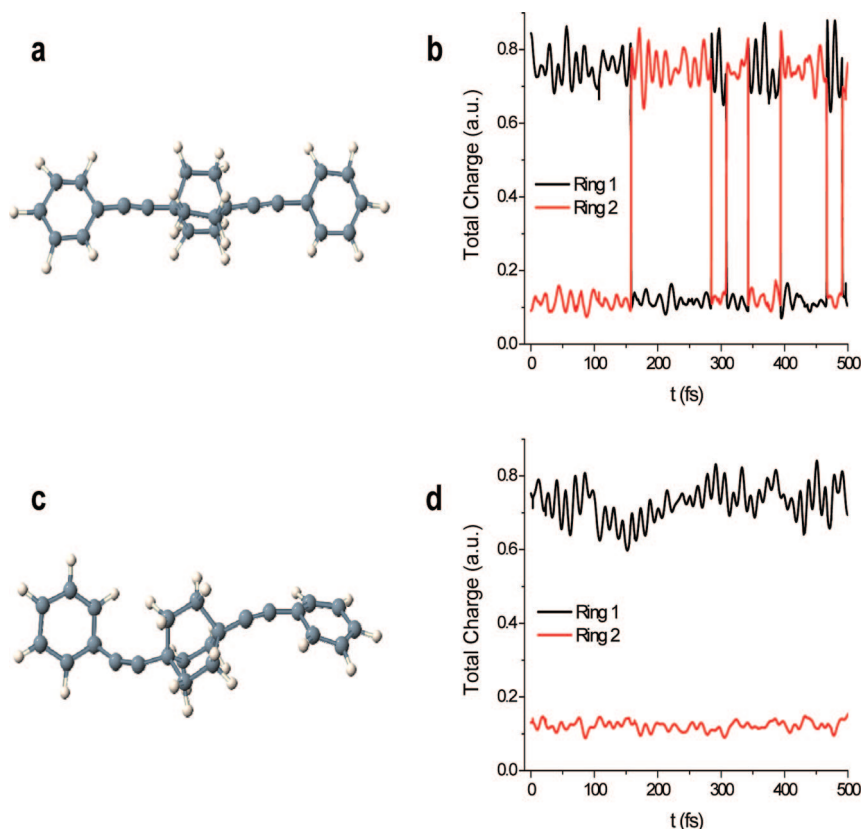
Figure 11. Charge transfer trajectories for a model of **1**$^+$ at different effective temperatures. (a) Molecular dynamics snapshot with zero point energy (0 K) in each of the modes and the corresponding trajectory (b) showing charge shift. (c) A molecular dynamics snapshot after equilibration at 300 K with (d) no charge shift in the trajectory.

validity requires a high E_i/V_{ij} ratio, can also be significantly overestimating the reduction. However use of the semiclassical Marcus equation in the nonadiabatic limit,

$$k_{CS} = \frac{2\pi}{\hbar} V_{eff}^2 \sqrt{\frac{1}{4\pi\lambda k_B T}} \exp\left(\frac{-\Delta G^\ddagger}{k_B T}\right) \quad (3)$$

with $\Delta G^\ddagger = (\lambda + \Delta G_{RP})^2/4\lambda$ and the parameters in Tables 1 and 2 suggest a V_{eff} in the range of several meV. Using eq 1 with this V_{eff} and the above E_i suggests a microscopic V_{ij} in the range of tens of meV, a range where eq 1 should be valid.

The NBO analysis predicts a significant change in V_{eff} upon benzo-annulation as a result of the changing hybridization and many interfering pathways within each rung, while our experimental results suggest a single dominant pathway that is unaffected by the change in hybridization. One way to achieve a dominant pathway relies on the interference between different orbitals within the σ-system (whether it be constructive or destructive) being destroyed by electronic dephasing, leaving one dominant pathway. Contributions from multiple spatial pathways require well-defined phase relationships of the charge carrier wave function to be maintained at all sites along the multiple pathways. The fidelity of this phase relationship can be conveniently expressed as the off-diagonal element (coherence) of the density matrix. Fluctuations in site energies (as well as intersite coupling) that exist at finite temperature can destroy these phase relationships[75,76] and spoil the legitimacy

of summing pathways coherently.[27,28,77] However, these fluctuations must occur on a sufficiently fast time scale to influence the additivity of the different pathways. A convenient method of estimating this time threshold is by calculating the Landauer–Büttiker tunneling time,[78] a concept adapted for Donor–Bridge–Acceptor molecules by Nitzan and co-workers[79] and shown in eq 4,

$$\tau_{tun} = \frac{\hbar N}{\Delta E} \quad (4)$$

where N is the number of bridge sites and ΔE is the energetic gap between the bridge and the D and A. Conceptually, this is the time scale at which bridge fluctuations must occur in order to influence the charge carrier using the bridge. When the transfer occurs via superexchange (large gap), these fluctuations must be incredibly fast in order to influence the charge carrier. This is consistent with the charge carrier never actually occupying the bridge and being consequently decoupled from its fluctuation. On the other hand, charge transfer operating with small gaps or in the hopping regime should be responsive to relatively slow fluctuations, since the actual occupation of the bridge makes the charge carrier more sensitive to fluctuations. With a gap of 1.9 eV (as estimated from the ionization potentials of BCO, 9.7 eV,[66] and CA, 7.8 eV[74]), the corresponding tunneling times of 0.3 fs suggest that if any interference did

(75) Skinner, J. L.; Hsu, D. *J. Phys. Chem.* **1986**, *90* (21), 4931.
(76) Onuchic, J. N.; Wolynes, P. G. *J. Phys. Chem.* **1988**, *92* (23), 6495.

(77) Skourtis, S. S.; Waldeck, D. H.; Beratan, D. N. *J. Phys. Chem. B* **2004**, *108* (40), 15511.
(78) Büttiker, M.; Landauer, R. *Phys. Rev. Lett.* **1982**, *49* (23), 1739.
(79) Nitzan, A.; Jortner, J.; Wilkie, J.; Burin, A. L.; Ratner, M. A. *J. Phys. Chem. B* **2000**, *104* (24), 5661.

exist, it would survive the electronic dephasing. Thus, dephasing should not erase interference in this case to leave a single dominant pathway.

The remaining alternative explanation simply restates that NBO analysis, though significantly informative in relating experimental observables to physical organic concepts,[63] is ultimately qualitative in nature. The importance of looking beyond nearest neighbors has been consistently shown through NBO calculations,[10,11,62] but the dominance of a single interaction may be overlooked by the NBO analysis. In this case, that single interaction would necessarily not involve the central σ bond (NBO 3), and would preserve the model in Figure 9.

MTHF Data at 300 K. Greater insight into the charge transfer mechanism may also be obtained by shifting to different solvents and temperatures. CS rates in MTHF show an increase over the toluene rates. This increase is consistent with the predictions of Marcus theory following the activation barriers in Table 1. In contrast to the charge separation rates in toluene, the rates measured in MTHF show a small but experimentally reproducible difference in rates with **1** and **4** being slightly faster than **2** and **3**. While we had initially viewed this difference in rates as a consequence of the altered σ-system, a more likely explanation can be drawn from the transient absorption spectra, Figure 6. While the spectra show only marginal differences in toluene, **1**–**4** show reproducible and relatively significant differences in MTHF. Since the ground-state absorption shows no difference among **1**–**4**, and the rates measured in toluene are essentially equivalent, the changes in rates and spectra in MTHF are likely attributed to changes in solvation of the ions in the radical pair.

Achieving the necessary solvent polarization is central to the Marcus theory of electron transfer,[60] comprising the critical reaction coordinate in the original formulation of the electron transfer reaction. The first and second solvent shells provide the critical stabilization for the shifting charges.[80,81] The additional bridge phenyl groups in **2**–**4** are located within the range of the first and second shells, and so we speculate that there will be a consequent disruption of the solvation shell. Such a steric disturbance of the solvent packing has previously been suggested to influence redox behavior.[82] Any differential solvation effect would be magnified in MTHF over toluene because of MTHF's higher dipole moment. That the rate does not vary monotonically with additional phenyl groups and the observation that it is the two 3-fold symmetric species that show the fastest rates suggest symmetry has a role maintaining optimal solvation. These systems would provide an interesting object of study for solvent molecular dynamics simulations. A similar nonmonotonic trend also suggesting the importance of symmetry was seen in the relative rates of bromine abstraction at the bridgehead position of a similar series of molecules.[83]

MTHF Data at 80 K. Evaluation of charge separation rates in a frozen glass serves two purposes. By reducing the population of high vibrational levels one can limit the conformational space explored by the molecule and learn about which conformations favor charge transfer. In addition, lowering the temperature may reduce the electronic dephasing rate enough to observe properties that rely on coherent summation of the charge carrier wave function over multiple spatially distinct parts of the molecule.[27,28] Despite frequently being referred to as rigid spacers, substituted alkynes can contort significantly at finite temperature.[84] Flexibility in D–B–A molecules can lead to the electronic properties being dominated by conformations other than the equilibrium one. This scenario was seen in molecules where charge transfer is symmetry-forbidden[85,86] and is elegantly captured in the simulations of Jones et al.[87]

The ground-state absorption spectra of **1** in MTHF are shown in Figure 10 at 300, 160, and 80 K. The sharpening of the features reveals two details about the system. First, though cyanoanthracene derivatives have been known to aggregate,[58,88] no aggregation occurs here as the absorption spectra show no evidence for the requisite exciton coupling[89] that accompanies aggregation.[90] Second, the reduction in inhomogeneous broadening suggests that the ensemble of molecules is adopting fewer different conformations. This is consistent with depopulation of excited conformational modes before solidification. The sharpened features imply that the conformations under study in the glass are closer to the equilibrium conformation than those in the solution phase.

Upon freezing, molecules **1**–**4** show monoexponential CS kinetics with significantly faster CS rates, although the reduced signal-to-noise may obscure the presence of additional components. Such behavior is reminiscent of the bacterial photosynthetic reaction center.[91,92] In that case the rate acceleration was explained as higher vibrations taking the system away from the bottom of the vibronic well, the optimal position for activationless charge transfer.[93] However, nonvanishing activation energies, Table 1, suggest this explanation is not valid in our system. More likely, the rise in CS rate is due to a conformational gating effect,[36,85,86,94] whereby the deviations from equilibrium conformation result in a reduction of V_{eff}. These less efficient conformations are accessed more frequently at 300 K than at 80 K. To test this hypothesis we followed the example of Jones and co-workers[95] and performed molecular dynamics coupled with semiempirical calculations to follow the charge transfer trajectories. Our simulated molecule is a model of **1** with a +1 charge, Figure 11. When only the zero-point energy was injected into the normal modes of the computational model system ($T = 0$ K), only geometries close to the equilibrium geometry were observed, Figure 11a, and a charge shift occurred within several hundred femtoseconds of the simulation, Figure 11b. In contrast, when additional energy was put into the system

(80) Barthel, E. R.; Martini, I. B.; Schwartz, B. J. *J. Phys. Chem. B* **2001**, *105* (49), 12230.

(81) Kuharski, R. A.; Bader, J. S.; Chandler, D.; Sprik, M.; Klein, M. L.; Impey, R. W. *J. Chem. Phys.* **1988**, *89* (5), 3248.

(82) Meier, M.; Sun, J.; Wishart, J. F.; van Eldik, R. *Inorg. Chem.* **1996**, *35* (6), 1564.

(83) Tabushi, I.; Yoshida, Z.; Aoyama, Y. *Bull. Chem. Soc. Jpn.* **1974**, *47* (12), 3079.

(84) Kelly, T. R. *Acc. Chem. Res.* **2001**, *34* (6), 514.

(85) Balzani, V.; Barigelletti, F.; Belser, P.; Bernhard, S.; De Cola, L.; Flamigni, L. *J. Phys. Chem.* **1996**, *100* (42), 16786.

(86) Zeng, Y.; Zimmt, M. B. *J. Am. Chem. Soc.* **1991**, *113* (13), 5107.

(87) Jones, G. A.; Paddon-Row, M. N.; Carpenter, B. K.; Piotrowiak, P. *J. Phys. Chem. A* **2002**, *106* (19), 5011.

(88) Morsi, S. E.; Carr, D.; El-Bayoumi, M. A. *Chem. Phys. Lett.* **1978**, *58* (4), 571.

(89) Kasha, M.; Rawls, H. R.; El-Bayoumi, M. A. *Pure Appl. Chem.* **1965**, *11*, 371.

(90) Acharya, S.; Bhattacharjee, D.; Talapatra, G. B. *Chem. Phys. Lett.* **2002**, *352* (5–6), 429.

(91) Fleming, G. R.; Martin, J. L.; Breton, J. *Nature* **1988**, *333* (6169), 190.

(92) Hoff, A. J.; Deisenhofer, J. *Phys. Rep.* **1997**, *287* (1–2), 2.

(93) Bixon, M.; Jortner, J. *J. Phys. Chem.* **1986**, *90* (16), 3795.

(94) Davis, W. B.; Ratner, M. A.; Wasielewski, M. R. *J. Am. Chem. Soc.* **2001**, *123* (32), 7877.

(95) Jones, G. A.; Carpenter, B. K.; Paddon-Row, M. N. *J. Am. Chem. Soc.* **1998**, *120* (22), 5499.

($T = 300$ K), the geometry deviated significantly from the equilibrium position, Figure 11c, and a charge shift was never observed, Figure 11d. These simulations confirm our hypothesis regarding the increased efficacy of the equilibrium conformation. An additional report detailing specific per-mode contributions is in progress.

The charge separation rate of **1** is seen to be marginally faster than **2**−**4**, although differences among **2**−**4** are difficult to probe due to degradation of the sample and the consequent size of the error bars. The relative steric bulk of **2**−**4** compared to **1** may also play a role in how the molecule interacts with the MTHF matrix. Since the trend here is loosely similar to that observed in solution and steric effects have been shown to be significant, the lower electronic dephasing rate due to the lower temperature is seen to be unimportant.

Conclusions

We have prepared a series of molecules to test the effect of additional π-pathways fused to a σ-scaffold on mediating electron transfer between two chromophores. Surprisingly, the π-pathways were shown to have no role in the electron transfer, and this situation was accurately captured by NBO analysis. Equally surprisingly, we found that the changes in the σ-system as a result of shifting hybridization also had no effect, despite the predictions of photoelectron spectra. We were able to suggest a series of relevant bonding orbitals that may be uninfluenced by the changing hybridization. However, we were unable to corroborate their dominance via NBO analysis possibly because of its own qualitative nature or because of the importance of electronic dephasing in effectively preventing the coherent addition of multiple σ-pathways. Charge separation rates in MTHF showed some differences between members of the series but were likely caused by differences in solvation. Charge separation rates increased at lower temperatures because the deviations from the equilibrium conformation experienced more severely at high temperatures decrease the electronic communication. This behavior was captured in molecular dynamics simulations coupled to semiempirical electronic structure calculations.

Supporting Information Available: Characterization of new molecules, synthetic procedures, sample calculations, cyclic voltammograms, full ref 37. This material is available free of charge via the Internet at http://pubs.acs.org.

JA8004623